Geophysical Research Letters

RESEARCH LETTER
10.1029/2021GL096868

Increased Variability of Biomass Burning Emissions in CMIP6 Amplifies Hydrologic Cycle in the CESM2 Large Ensemble

Kyle B. Heyblom[1], Hansi A. Singh[1], Philip J. Rasch[2,3], and Patricia DeRepentigny[4]

[1]School of Earth and Ocean Sciences, University of Victoria, Victoria, BC, Canada, [2]Pacific Northwest National Laboratory, Atmospheric Sciences and Global Change Division, U.S. DOE Office of Science, Richland, WA, USA, [3]Department of Atmospheric Science, University of Washington, Seattle, WA, USA, [4]Climate and Global Dynamics Laboratory, National Center for Atmospheric Research, Boulder, CO, USA

Abstract Historical simulations performed for the Coupled Model Intercomparison Project Phase 6 used biomass burning emissions between 1997 and 2014 containing higher spatial and temporal variability compared to emission inventories specified for earlier years, and compared to emissions used in previous (e.g., CMIP5) simulation intercomparisons. Using the Community Earth System Model version 2 Large Ensemble, we show this increased biomass burning emissions variability leads to amplification of the hydrologic cycle poleward of 40°N. Notably, the high variability of biomass burning emissions leads to increased latent heat fluxes, column-integrated precipitable water, and precipitation. Greater ocean heat uptake, weaker meridional energy transport from the tropics, greater atmospheric shortwave and longwave absorption, and lower relative humidity act to moderate this hydrologic cycle amplification. Our results suggest it is not only the secular changes (on multidecadal timescales) in biomass burning emissions that impact the hydrologic cycle, but also the shorter timescale variability in emissions.

Plain Language Summary Global climate models use different inputs to simulate the past climate as accurately as possible. One of these inputs is an estimate of emissions from the burning of biomass (e.g., from forests and cropland). In the sixth phase of the Climate Model Intercomparison Project Phase 6, the estimated biomass burning emissions were derived using two very different methods. Prior to 1997, emission estimates relied on a combination of indirect measurements and best-guess fire modeling resulting in emissions having relatively modest temporal and spatial variability. During later periods (i.e., 1997–2014) satellite based estimates of fire occurrence and intensity were used in combination with biogeochemical models to produce emission estimates containing much larger spatial and temporal variability. This study demonstrates that the differing variability in biomass burning has an impact on the model's water cycle. During years of strong burning episodes, clouds thin and more sunlight reaches the surface, which results in more surface evaporation, and higher atmospheric humidity and precipitation. Additionally, the high variation in emissions increases rainfall, decreases snowfall, and increases the intensity of extreme precipitation events. Our results show that the timing of biomass burning emissions, not just the amount emitted, is an important moderator of the atmospheric water cycle.

Key Points:

- Increased biomass burning emissions variability in Coupled Model Intercomparison Project Phase 6 amplifies hydrologic cycle in Community Earth System Model version 2
- Column-integrated precipitable water, evaporation, and precipitation all increase poleward of 40°N
- Several moderating factors act to mitigate hydrologic cycle amplification

Supporting Information:

Supporting Information may be found in the online version of this article.

Correspondence to:

K. B. Heyblom,
kheyblom@uvic.ca

Citation:

Heyblom, K. B., Singh, H. A., Rasch, P. J., & DeRepentigny, P. (2022). Increased variability of biomass burning emissions in CMIP6 amplifies hydrologic cycle in the CESM2 Large Ensemble. *Geophysical Research Letters*, *49*, e2021GL096868. https://doi.org/10.1029/2021GL096868

Received 3 NOV 2021
Accepted 9 FEB 2022

1. Introduction

Many factors affect the atmospheric hydrologic cycle, and aerosols are among the most important of these factors. Aerosols impact regional and global scale precipitation through their direct radiative forcing and indirect microphysical effects (e.g., see Boucher et al., 2013; Ramanathan et al., 2001, and references therein). Simulation of the hydrologic cycle in historical and future projections is highly dependent on accurate modeling of aerosols. Indeed, aerosol-cloud interactions and their associated radiative forcing are among the most uncertain components of the historical radiative forcing of Earth's climate (Boucher et al., 2013; Flato et al., 2013; Kiehl, 2007; Seinfeld et al., 2016).

While aerosols are a topic of great interest to the climate community, comparatively little attention has been directed to how the variability of aerosol emissions affect the climate system (rather than the total amount of such emissions). Current knowledge is mostly based on scenarios which are inherently idealized. For example, the latest Geoengineering Model Intercomparison Project Phase 6 (Kravitz et al., 2015) experiments prescribe aerosol emissions as either constant in time, increasing at a fixed rate, or as an instantaneous change. Many others

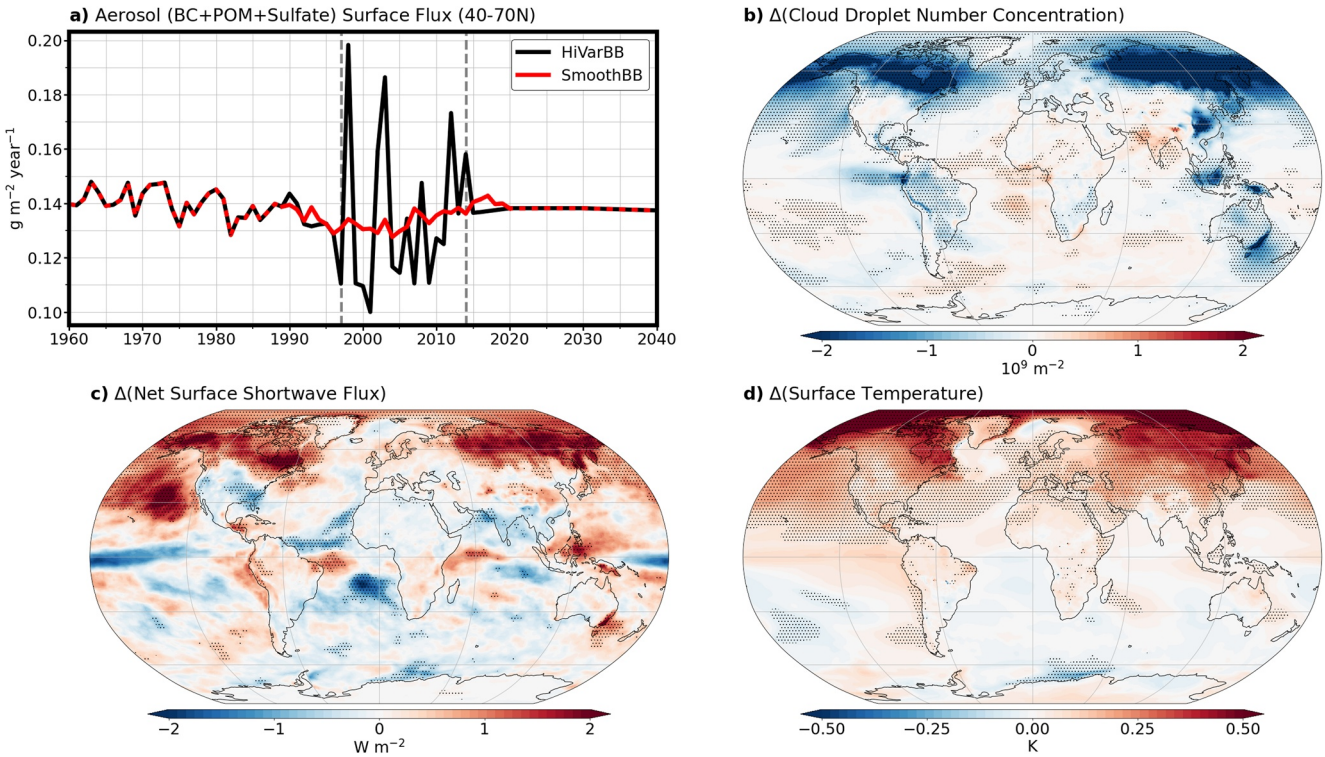

Figure 1. Aerosol emission scenarios and resulting differences in cloud and radiative responses. Panel (a) shows the annual mean sum of black carbon, primary organic, and sulfate aerosol surface fluxes from HiVarBB (black line) and SmoothBB (red line) ensemble sets averaged from 40° to 70°N, with the vertical gray dashed lines delineating the Global Fire Emissions Database (GFED) period (1997–2014). Panels (b–d) show ensemble mean differences (average of HiVarBB ensemble members minus average of SmoothBB ensemble members) in (b) vertically integrated cloud droplet number concentration, in 10^9 m^{-2}; (c) net surface shortwave flux, in W m^{-2}; and (d) surface temperature, in K, during the GFED period (1997–2014). Stippling signifies 95% confidence in the significance of the difference between ensemble member sets (see Text S1 in Supporting Information S1).

have used instantaneous change approaches to study the precipitation response to aerosols (e.g., see Andrews et al., 2010; Kvalevåg et al., 2013; Ming et al., 2010; Richardson et al., 2016). Fast and slow precipitation responses (e.g., see Andrews et al., 2009; Bala et al., 2010) to aerosols were evaluated in the Precipitation Driver and Response Model Intercomparison Project (Myhre et al., 2017; Samset et al., 2016) using a single instantaneous change in both black carbon and sulfate aerosol concentrations. Both the Model Intercomparison Project on the climatic response to volcanic forcing (Zanchettin et al., 2016) and the fourth phase of the Paleoclimate Model Intercomparison Project (Jungclaus et al., 2017) simulate the effect of volcanic emissions, which are necessarily episodic. However, the volcanic events simulated in these experiments are large and occur infrequently (i.e., they are years to decades apart). None of the above studies explore the climate impact of interannual emissions variability, or compare the impacts of variable aerosol emissions to continuous emissions.

Unlike the emissions used in many previous intercomparison activities, the biomass burning emissions prescribed for the sixth phase of the Climate Model Intercomparison Project Phase 6 (CMIP6) historical simulations (BB4CMIP6; see van Marle et al., 2017) contain separate periods characterized by low and high interannual variability, thereby providing an opportunity to explore how such variability impacts the climate system. The methods and measurements used to construct this aerosol emission inventory utilized a variety of strategies over different intervals within the historical period (1850–2014) that produce different variability in estimated emissions. Between 1997 and 2014, the Global Fire Emissions Database version 4 with small fires (hereafter GFED; van der Werf et al., 2017) was used to estimate biomass burning emissions. These estimates include much higher temporal variability compared to prior years. Similar strategies were used for other aerosol sources (Hoesly et al., 2018). The interannual variability of black carbon, sulfate, and primary organics emitted between 40° and 70°N during 1997–2014 is approximately six times greater than the 18 years prior to it (as assessed from the standard deviation; see Figure 1a, black line). This large change in variability is new to the CMIP6 forcing

and was not present in CMIP5, where decadal means were used to construct historical gridded biomass burning emissions (Lamarque et al., 2010). The prescribed biomass burning emissions largely consist of primary aerosols and reactive gases (van Marle et al., 2017), many of which result in the formation of secondary organic aerosols (Pandis et al., 1992).

Recent studies by DeRepentigny et al. (2022) and Fasullo et al. (2022) have compared the climate impacts of these (high variability) BB4CMIP6 emissions with simulations using emissions with less variability. Both studies find that it is not only the magnitude of aerosol emissions that impact the climate system, but also their temporal variability. Fasullo et al. (2022) showed that the sudden increase in aerosol emissions variability from 1997 to 2014 acts to decrease cloud droplet number concentrations (CDNCs) and low cloud amount, which increases downwelling shortwave radiation. DeRepentigny et al. (2022) further showed that greater variability in biomass burning emissions accelerated Arctic sea ice loss over this time period. Given that aerosols have a profound impact on the hydrologic cycle, a natural question that arises is the following: how does such a change in the temporal variability of biomass burning emissions affect the hydrologic cycle?

This study addresses this very question. Following the findings of DeRepentigny et al. (2022) and Fasullo et al. (2022), the Community Earth System Model version 2 Large Ensemble Community Project (CESM2-LE; Rodgers et al., 2021) forced half of its ensemble members with the original CMIP6 biomass burning emissions, and the second half with smoothed biomass burning emissions during the period of increased variability (from 1997 to 2014; Figure 1a, red line). Here, we utilize these two sets of simulations to investigate the impact that this increase in biomass burning emissions variability has on the global atmospheric hydrologic cycle. We find the high variability of biomass burning emissions amplifies the atmospheric hydrologic cycle, defined here as increased evaporation, column-integrated precipitable water, and precipitation. Conversely, we find that several moderating factors act to mitigate this amplification of the hydrologic cycle. We conclude with a discussion of the implications of our findings for research utilizing CMIP6 output over the historical period.

2. Model Data

We assess the impact of biomass burning emissions variability on the atmospheric hydrologic cycle using the CESM2-LE (Rodgers et al., 2021). This large ensemble project used the fully coupled CESM2 configured with the Community Atmosphere Model version 6 (Danabasoglu et al., 2020), Parallel Ocean Program version 2 (Smith et al., 2010), Los Alamos Sea Ice Model version 5.1.2 (Hunke et al., 2015), and Community Land Model version 5 (Lawrence et al., 2019). Aerosols were simulated using the four-mode version of the Modal Aerosol Module (Liu et al., 2016). Each component was configured at a nominal 1° spatial resolution (Rodgers et al., 2021).

We analyze 80 CESM2-LE ensemble members subject to historical emissions (1850–2014) and the future SSP3-7.0 emissions (a medium-to-high emission scenario from 2015 to 2100; see O'Neill et al., 2016). Half of these 80 members were forced with the standard CMIP6 biomass burning emissions (hereafter HiVarBB; Figure 1a, black line; van Marle et al., 2017). The other half instead used a temporally smoothed biomass burning emission inventory (hereafter SmoothBB; Figure 1a, red line). This temporal smoothing was achieved by using an 11-year running mean filter from 1990 to 2020. This smoothing method reduced the interannual variability such that it aligned more closely with the variability of biomass burning emissions before the GFED period (1997–2014), but still nearly preserved the total cumulative amount of aerosol emissions through this period. Because fires varied from one year to another, the temporally smoothed emission inventory is also spatially smoother. The 80 members were initialized from four different years of the pre-industrial control simulation (years 1231, 1251, 1281, and 1301). Each initialization year was selected based on the phase of the Atlantic Meridional Overturning Circulation strength (see Rodgers et al., 2021). Twenty members were started from each initialization year by randomly perturbing the temperature field. Half of each 20 member set used the HiVarBB emissions, while the other half used the SmoothBB emissions. In addition to differences in biomass burning emissions variability, the two ensemble member sets were forced with slight differences in SO_4 and SOAG emissions and CO_2 uptake which were the result of small bug corrections. These differences were determined to be too small to have an effect on climate results (Rodgers et al., 2021). We evaluate the relative impact of the increase in biomass burning variability by comparing the HiVarBB and SmoothBB simulations over the GFED period (1997–2014).

3. Cloud and Surface Radiative Response

In the CESM2-LE, the choice of biomass burning emissions (HiVarBB or SmoothBB; Figure 1a, black and red lines, respectively) impacts clouds and surface radiation. CDNCs are lower in ensemble members subjected to the CMIP6 biomass burning emissions relative to those subjected to the smoothed biomass burning emissions during the GFED period (i.e., the average of HiVarBB ensemble members minus the average of the SmoothBB ensemble members from 1997 to 2014; Figure 1b). The difference in CDNC is particularly large over the North American and Asian boreal forest regions. This time-integrated change in CDNC is likely due to a nonlinearity in CDNC response to aerosol emissions (as described by Carslaw et al. (2013)). This cloud thinning effect in HiVarBB ensemble members, relative to SmoothBB ensemble members, leads to greater surface absorption of shortwave radiation (Figure 1c; see also DeRepentigny et al., 2022; Fasullo et al., 2022). This larger net surface shortwave radiation leads to surface warming in HiVarBB ensemble members relative to SmoothBB ensemble members during the GFED period (Figure 1d).

4. Hydrologic Cycle Response

We find that the hydrologic cycle amplifies when biomass burning emissions variability is high during the GFED period. Surface latent heat fluxes are greater in HiVarBB ensemble members compared to SmoothBB ensemble members over most of the area poleward of 40°N (Figure 2a). In general, regions with greater latent heat fluxes correspond to those that experience more surface shortwave heating (compare spatial patterns of net surface shortwave flux differences and latent heat flux differences in Figures 1c and 2a, respectively). These areas with larger latent heat flux are expected as more energy at the surface is available for evaporation (Peixoto & Oort, 1992). Poleward of 40°N, the surface latent heat flux is 0.8% (0.3 W/m^2) larger in the HiVarBB ensemble members compared to the SmoothBB ensemble members during the GFED period (Figure 2b and Figure S1a in Supporting Information S1).

These greater latent heat fluxes in the HiVarBB simulations are accompanied by greater column-integrated precipitable water over most of the Northern Hemisphere (NH) relative to the SmoothBB simulations (Figure 2c). Regional differences are statistically significant over most regions of the NH and all regions north of 30°N. Poleward of 40°N, the area-averaged column-integrated precipitable water is 1.4% (0.2 kg/m^2) larger in the HiVarBB simulations relative to the SmoothBB simulations (Figure 2d), a difference that is statistically significant (Figure S1b in Supporting Information S1). This difference corresponds to a 5.7% increase in water vapor per Kelvin of surface air warming, a rate smaller than expected from the Clausius–Clapeyron scaling factor of ∼7%/K (e.g., Held & Soden, 2006; Trenberth et al., 2003). This weaker scaling is likely driven by a reduction in relative humidity (RH; O'Gorman & Muller, 2010, also see Section 5).

Consistent with greater evaporation and atmospheric precipitable water, the HiVarBB emissions also increase precipitation over most regions poleward of 40°N relative to the SmoothBB emissions (Figure 2e). When averaged poleward of 40°N, greater precipitation in the HiVarBB simulations is clear (Figure 2f) and statistically significant (Figure S1c in Supporting Information S1). Specifically, total precipitation poleward of 40°N is 0.5% (0.01 mm/day) greater in the HiVarBB simulations relative to the SmoothBB simulations during the GFED period. Greater precipitation is expected with higher surface temperatures that arise from greater net surface shortwave fluxes (e.g., Allen & Ingram, 2002; Andrews et al., 2009).

There is also a discernible northward shift in the Inter-Tropical Convergence Zone (ITCZ) in the HiVarBB simulations relative to the SmoothBB simulations (in agreement with Broccoli et al. (2006), and described further in Section 5). This is apparent in Figure 2e as a statistically significant northward ITCZ shift over the Atlantic Ocean and drying of the South Pacific Convergence Zone.

Higher surface temperatures in the NH in the HiVarBB simulations relative to SmoothBB simulations also leads to a shift in precipitation phase. In the NH high latitudes, a larger fraction of precipitation falls as rain rather than snow in HiVarBB ensemble members relative to SmoothBB ensemble members (Figure 2g). Regional differences in the relative amount of liquid precipitation (proportion of liquid to total precipitation) are statistically significant over much of the NH high latitudes. Averaged poleward of 40°N over the GFED period, the proportion of precipitation that falls as rain is 0.8% larger in the HiVarBB ensemble members relative to the SmoothBB ensemble members (Figure 2h) and is statistically significant (Figure S1d in Supporting Information S1). This

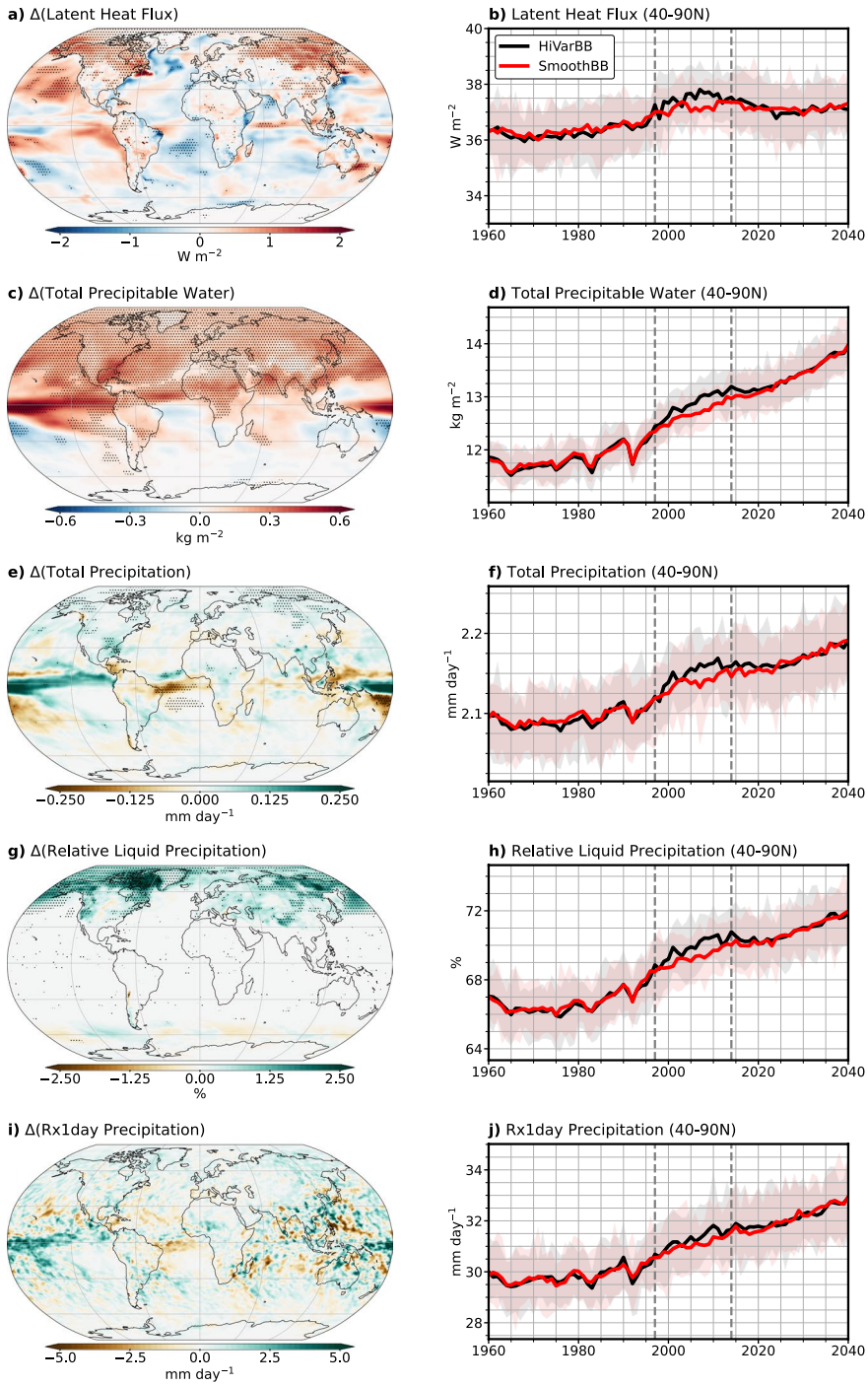

Figure 2. Differences in the atmospheric hydrologic cycle. (a and b) Latent heat flux, in W m^{-2}; (c and d) column-integrated precipitable water, in kg m^{-2} (e and f) total precipitation, in mm day^{-1}; (g and h) percentage of precipitation that is liquid; and (i and j) annual maximum daily precipitation (Rx1day) in mm day^{-1}. The left column shows the ensemble mean difference (average of HiVarBB ensemble members minus average of SmoothBB ensemble members), with stippling signifying 95% confidence (see Text S1 in Supporting Information S1). The right column shows the annual mean value, averaged from 40° to 90°N, in HiVarBB (black line) and SmoothBB (red line) ensemble members; thick lines denote the ensemble mean, shading denotes the range of each ensemble member set, and vertical gray dashed lines delineate the Global Fire Emissions Database period (1997–2014).

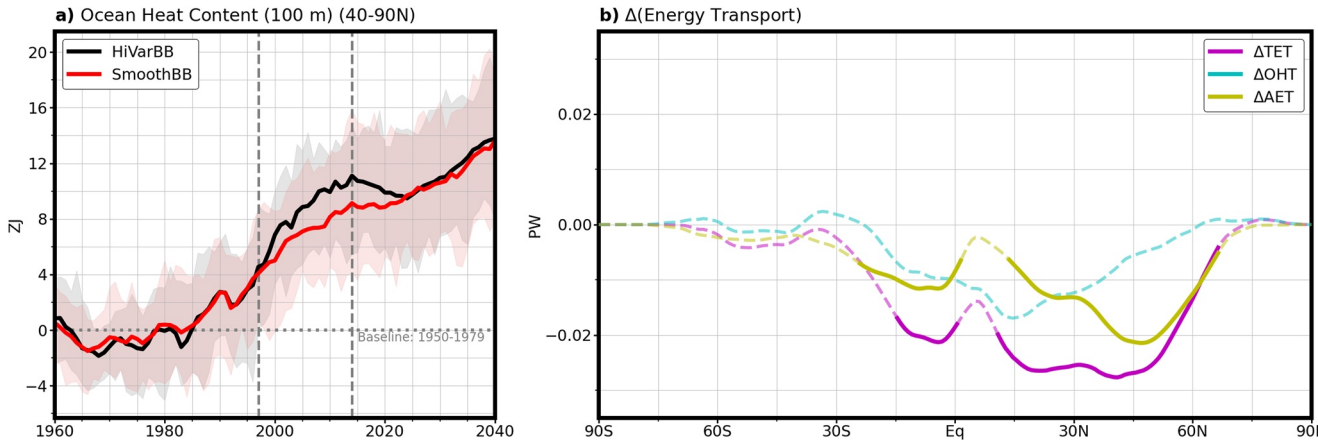

Figure 3. Energetic limitations on hydrologic cycle amplification. (a) Upper (top 100 m) ocean heat content anomalies relative to the 1950–1979 average from 40° to 90°N in HiVarBB (black line) and SmoothBB (red line) simulations, in ZJ; and (b) ensemble mean difference (average of HiVarBB ensemble members minus average of SmoothBB ensemble members) in the meridional northward energy transport during the Global Fire Emissions Database period (1997–2014), in PW, including total (ΔTET; black line), atmosphere (ΔAET; yellow line), and ocean (ΔOHT; cyan line) components. In panel (a), thick lines denote the ensemble mean, while shading denotes the range of each member set. In panel (b), solid lines signify 95% confidence in the significance of the difference between HiVarBB and SmoothBB ensemble member sets (see Text S1 in Supporting Information S1).

shift in precipitation phase is present in all seasons, but most apparent during boreal summer (JJA; Figure S2 in Supporting Information S1).

We also find the annual maximum daily precipitation is larger in the HiVarBB simulations compared to SmoothBB simulations over the GFED period for most regions poleward of 40°N. Unlike total precipitation, there is no statistical significance in regional differences in annual maximum daily precipitation (Figure 2i). However, there is statistical significance in the 40°–90°N mean difference during the GFED period. Specifically, the annual maximum daily precipitation is 0.7% (0.2 mm/day) larger in the HiVarBB simulations relative to SmoothBB simulations (Figure 2j), and this difference is statistically significant (Figure S1e in Supporting Information S1). Greater intensity of extreme precipitation events in HiVarBB ensemble members compared to SmoothBB ensemble members is generally consistent with greater precipitable water (Allen & Ingram, 2002; Trenberth et al., 2003) and more surface warming (Utsumi et al., 2011).

5. Moderating Factors to Hydrologic Cycle Amplification

As we have shown, the hydrologic cycle is sensitive to biomass burning emissions variability. However, other compensating ocean and atmospheric processes act to moderate the extent to which increased biomass burning emissions variability amplifies the hydrologic cycle. Most notably, larger ocean heat storage and weaker meridional energy convergence constrain evaporation increases poleward of 40°N. At the same time, changes in atmospheric absorption of shortwave radiation and RH reduce precipitation efficiency in the HiVarBB simulations, which act to constrain precipitation increases.

First, greater ocean heat storage in HiVarBB simulations moderates hydrologic cycle amplification (Figure 3a). Poleward of 40°N, upper ocean heat content (from 0 to 100 m depth) is 1.6 ZJ larger in the HiVarBB simulations compared to the SmoothBB simulations during the GFED period, a difference which is statistically significant (Figure S3b in Supporting Information S1). With greater ocean heat storage, not all surplus energy input (from greater surface shortwave radiative fluxes, as shown in Figure 1c) immediately goes to increasing evaporative fluxes, thereby moderating their rise. Greater upper ocean heat content in HiVarBB simulations persists for approximately 10 years after the end of the GFED period, indicating that ocean heat storage both moderates and lengthens the time scale of the climate response (as described by Barsugli and Battisti (1998)).

Adjustments in meridional energy transport further mitigate hydrologic cycle differences poleward of 40°N between HiVarBB and SmoothBB simulations. Figure 3b shows the difference in energy transport between the two simulation ensemble sets, including total, atmosphere, and ocean components. NH total energy transport is lower in HiVarBB simulations relative to SmoothBB simulations (Figure 3b, black line) during the GFED

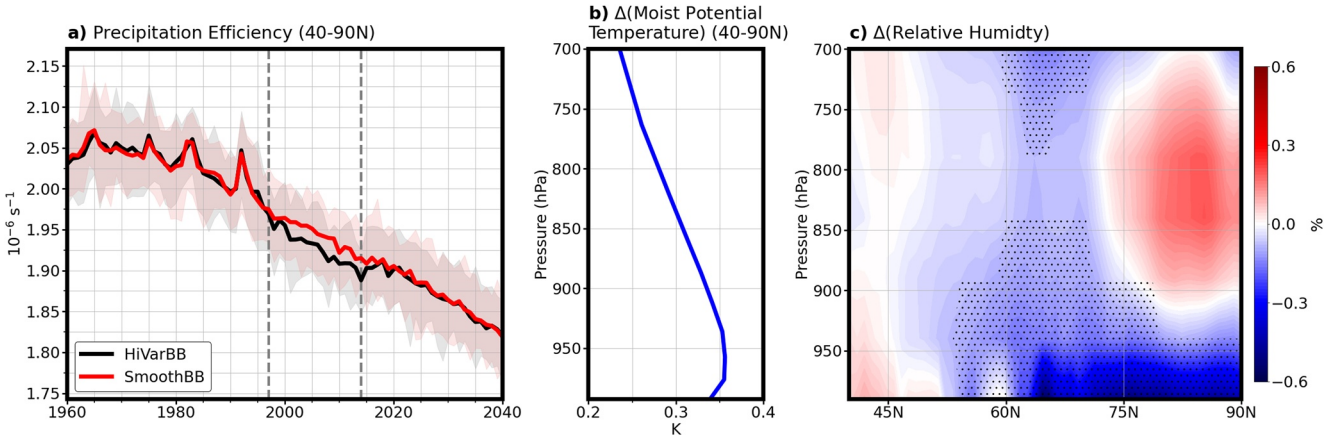

Figure 4. Precipitation efficiency and factors that impact it. (a) Total precipitation efficiency, in 10^{-6} s^{-1}, in HiVarBB (black line) and SmoothBB (red line) simulations, with the vertical gray dashed lines delineating the Global Fire Emissions Database (GFED) period (1997–2014); (b) ensemble mean difference in the mean 40°–90°N vertical moist potential temperature profile, in K; and (c) ensemble mean difference in zonal mean relative humidity from 40° to 90°N, in %. In panel (a), thick lines denote the ensemble mean, while the shaded regions denote the range of each ensemble member set. In panels (b and c), the ensemble mean differences are computed as the average of HiVarBB ensemble members minus the average of SmoothBB ensemble members during the GFED period (1997–2014). In panel (b), the solid line signifies 95% confidence in the significance of the difference between ensemble member sets (see Text S1 in Supporting Information S1). In panel (c), stippling signifies 95% confidence in the significance of the difference between ensemble member sets (see Text S1 in Supporting Information S1).

period. This lower energy transport is a response to greater energy input poleward of 40°N (Figure 1c), which tends to flatten the meridional moist static energy gradient and thereby weaken energy transport (Hwang & Frierson, 2010). Indeed, the total atmospheric energy transport is weaker in HiVarBB simulations compared to SmoothBB simulations (Figure 3b, yellow line). This anomalously southward atmospheric energy transport is consistent with a stronger Southern Hemisphere Hadley Cell in HiVarBB simulations (see dry and moist components of atmospheric energy transport in Figure S5 in Supporting Information S1) which drives the ITCZ further north (recall Figure 2e) and increases net southward atmospheric energy transport in the deep tropics (see Broccoli et al., 2006; Kang et al., 2008). Likewise, lower ocean heat transport also contributes to weaker NH total energy transport (Figure 3b, cyan line). Although the lower ocean heat transport is not statistically significant, the weakening of the Atlantic Meridional Ocean Circulation is significant (Figure S6 in Supporting Information S1), indicating a decline in ocean heat transport in the Atlantic basin. Weaker meridional energy transport in HiVarBB simulations reduces the energy available for surface warming and evaporation, thereby moderating hydrologic cycle amplification.

Despite greater total precipitation in the HiVarBB simulations, the precipitation efficiency (defined here as the ratio of precipitation to column-integrated precipitable water evaluated locally) is lower in HiVarBB simulations relative to SmoothBB simulations (Figure 4a). The average precipitation efficiency poleward of 40°N is 0.9% (1.7×10^{-8} s^{-1}) lower in HiVarBB ensemble members compared to SmoothBB ensemble members, a difference that is statistically significant (Figure S3a in Supporting Information S1). Lower precipitation efficiency means that the atmosphere is less able to precipitate the moisture that is contained within it. Three mechanisms act to lower precipitation efficiency in the HiVarBB simulations relative to the SmoothBB simulations. First, greater atmospheric black carbon aerosol burdens and atmospheric water vapor in the HiVarBB simulations result in greater atmospheric absorption of shortwave radiation (Figures S4a–S4c in Supporting Information S1), which acts to reduce condensation (Mitchell et al., 1987; O'Gorman et al., 2012; Previdi, 2010), and also increases static stability in the lower troposphere (by increasing moist potential temperature between 990 and 950 hPa; see Figure 4b). Greater static stability in HiVarBB simulations acts to suppress vertical motion and cloud formation relative to the SmoothBB simulations (consistent with O'Gorman and Schneider (2009) and Richter and Xie (2008)). Second, greater upper tropospheric water vapor (see Figure S4b in Supporting Information S1) decreases atmospheric radiative cooling (Allen & Ingram, 2002; Previdi, 2010). Third, because lower tropospheric RH is lower poleward of 40°N in the HiVarBB simulations (Figure 4c), more energy is required to raise air parcels to their lifting condensation level relative to the SmoothBB simulations. Additionally, air parcels are less likely to be lifted to levels where they can saturate, as the atmosphere is more statically stable in the HiVarBB simulations (Wallace & Hobbs, 2006). This lower RH is likely caused by water limitations over land, where the

largest differences in surface shortwave absorption and surface temperature occur (Figures 1c and 1d; O'Gorman & Muller, 2010).

6. Implications

Our results provide clear evidence that variability in biomass burning emissions affect the hydrologic cycle. We show that greater biomass burning emissions variability, as used in CMIP6 historical simulations during the GFED period (1997–2014), amplifies the hydrologic cycle in CESM2. Evaporation, atmospheric precipitable water, mean precipitation, precipitation extremes, and fraction of rain precipitation all increase with greater biomass burning emissions variability. This amplification is consistent with the thermodynamic impact of warming (e.g., Allen & Ingram, 2002; Held & Soden, 2006; Stott et al., 2010). Conversely, this hydrologic cycle amplification is moderated by several competing factors: greater ocean heat storage moderates the available energy for evaporation over ocean; weaker meridional energy transport decreases the energy available for surface warming; and greater atmospheric radiative absorption and lower RH in HiVarBB ensemble members leads to lower precipitation efficiency poleward of 40°N.

It is possible these findings extend to other models participating in CMIP6, not just CESM2. All CMIP6 historical simulations use the same biomass burning emissions, including the increase in variability during the GFED period. Indeed, Fasullo et al. (2022) and DeRepentigny et al. (2022) find evidence of characteristic increases in downwelling shortwave radiation and Arctic sea ice loss, respectively, during the GFED period in several other CMIP6 models. This suggests that other models may also be sensitive to greater biomass burning emissions variability. Further care is required for future treatments of biomass burning emissions variability in historical simulations. If the biomass burning emissions variability over the entire historical and future projection periods was corrected to be more continuous (whether to align with the variability of the GFED estimates, or the estimates prior), the hydrologic cycle would likely change. We note, however, that although each model is subject to the same increase in variability, this does not mean that every model is sensitive to this change (DeRepentigny et al., 2022; Fasullo et al., 2022). We also note that differing model sensitivities to this variability may increase the inter-model spread, and therefore uncertainty, over the GFED period. This highlights the need for further study into how greater biomass burning variability during the GFED period affects hydrologic cycle in a range of CMIP6 models. To assess whether the results presented here from CESM2 are robust, it would be appropriate to run similar modeling experiments using other CMIP6 Earth system models.

As indicated by these findings, care is required when analyzing hydrologic cycle fields within CMIP6 and CESM2-LE historical simulations. Precipitation robustly increases in most areas poleward of 40°N in CMIP6 future projections (Cook et al., 2020). If a baseline includes the GFED period (1997–2014), precipitation increases over future time periods are likely to be computed as lower than if adjacent baseline periods are used. For example, the change in mean precipitation poleward of 40°N from 1995–2015 to 2080–2100 is approximately 7% smaller in the HiVarBB simulations than the SmoothBB simulations. Furthermore, the difference in precipitation between HiVarBB and SmoothBB simulations during the GFED period represents 6% of the total mean precipitation signal between 1950–1980 to 2070–2100 in CESM2. Similar issues are likely even worse for other hydrologic cycle variables, such as atmospheric water vapor, as the relative difference between HiVarBB and SmoothBB simulations is even larger. As such, this study highlights a previously unknown source of uncertainty in hydrologic cycle projections.

Our findings demonstrate that the interannual variability of biomass burning emissions may be an important factor that determines the strength of the atmospheric hydrologic cycle. More research is required to better understand the mechanisms driving the climate response to biomass burning emissions variability, particularly that of aerosols and aerosol-adjacent compounds. We underscore the need for studies using multiple models to better parse out the underlying mechanisms by which biomass burning emissions variability impacts the hydrologic cycle and the greater climate system.

Data Availability Statement

This material is based upon work supported by the National Center for Atmospheric Research (NCAR). CESM2-LE data are available here https://www.cesm.ucar.edu/projects/community-projects/LENS2/. Information on the release of the CESM2-LE is available here https://doi.org/10.5194/esd-12-1393-2021.

Acknowledgments
K. B. Heyblom was supported by the Natural Sciences and Engineering Council of Canada (NSERC), the Province of British Columbia, and the University of Victoria. H. A. Singh was supported by base research support through the University of Victoria. P. J. Rasch was supported by the Pacific Northwest National Laboratory (PNNL) which is operated for DOE by the Battelle Memorial Institute under contract DE-AC05-76RL01830. P. DeRepentigny was supported by the Advanced Study Program of the National Center for Atmospheric Research (NCAR), which is a major facility sponsored by the National Science Foundation (NSF) under Cooperative Agreement No. 1852977. All authors would like to acknowledge the CESM2 Large Ensemble Community Project and supercomputing resources provided by the IBS Center for Climate Physics in South Korea. The CESM project was supported by the National Center for Atmospheric Research (NCAR), which is a major facility sponsored by the NSF under Cooperative Agreement No. 1852977.

References

Allen, M. R., & Ingram, W. J. (2002). Constraints on future changes in climate and the hydrologic cycle. *Nature*, *419*(6903), 228–232. https://doi.org/10.1038/nature01092

Andrews, T., Forster, P. M., Boucher, O., Bellouin, N., & Jones, A. (2010). Precipitation, radiative forcing and global temperature change. *Geophysical Research Letters*, *37*(14). https://doi.org/10.1029/2010GL043991

Andrews, T., Forster, P. M., & Gregory, J. M. (2009). A surface energy perspective on climate change. *Journal of Climate*, *22*(10), 2557–2570. https://doi.org/10.1175/2008JCLI2759.1

Bala, G., Caldeira, K., & Nemani, R. (2010). Fast versus slow response in climate change: Implications for the global hydrological cycle. *Climate Dynamics*, *35*(2–3), 423–434. https://doi.org/10.1007/s00382-009-0583-y

Barsugli, J. J., & Battisti, D. S. (1998). The basic effects of atmosphere–ocean thermal coupling on midlatitude variability. *Journal of the Atmospheric Sciences*, *55*(4), 477–493. https://doi.org/10.1175/1520-0469(1998)055<0477:TBEOAO>2.0.CO;2

Boucher, O., Randall, D., Artaxo, P., Bretherton, C., Feingold, G., Forster, P., et al. (2013). Chapter 7: Clouds and aerosols. In *Climate Change 2013: The Physical Science Basis. Contribution of Working Group I to the Fifth Assessment Report of the Intergovernmental Panel on Climate Change* (pp. 571–658). https://doi.org/10.1017/CBO9781107415324.016

Broccoli, A. J., Dahl, K. A., & Stouffer, R. J. (2006). Response of the ITCZ to Northern Hemisphere cooling. *Geophysical Research Letters*, *33*(1). https://doi.org/10.1029/2005GL024546

Carslaw, K. S., Lee, L. A., Reddington, C. L., Pringle, K. J., Rap, A., Forster, P. M., et al. (2013). Large contribution of natural aerosols to uncertainty in indirect forcing. *Nature*, *503*(7474), 67–71. https://doi.org/10.1038/nature12674

Cook, B. I., Mankin, J. S., Marvel, K., Williams, A. P., Smerdon, J. E., & Anchukaitis, K. J. (2020). Twenty-first century drought projections in the CMIP6 forcing scenarios. *Earth's Future*, *8*(6). https://doi.org/10.1029/2019EF001461

Danabasoglu, G., Lamarque, J. F., Bacmeister, J., Bailey, D. A., DuVivier, A. K., Edwards, J., et al. (2020). The Community Earth System Model Version 2 (CESM2). *Journal of Advances in Modeling Earth Systems*, *12*(2). https://doi.org/10.1029/2019MS001916

DeRepentigny, P., Jahn, A., Holland, M., Kay, J., Fasullo, J., Lamarque, J.-F., et al. (2022). Enhanced simulated early 21st century Arctic sea ice loss due to CMIP6 biomass burning emissions. *Earth and Space Science Open Archive*, 1–42. https://doi.org/10.1002/essoar.10510652.1

Fasullo, J. T., Lamarque, J.-F., Hannay, C., Rosenbloom, N., Rosenblum, N., Tilmes, S., et al. (2022). Spurious late historical-era warming in CESM2 and other CMIP6 climate simulations driven by prescribed biomass burning emissions. *Geophysical Research Letters*, *49*(2). https://doi.org/10.1029/2021GL097420

Flato, G., Marotzke, J., Abiodun, B., Braconnot, P., Chou, S., Collins, W., et al. (2013). Chapter 9: Evaluation of climate models. In *Climate Change 2013: The Physical Science Basis. Contribution of Working Group I to the Fifth Assessment Report of the Intergovernmental Panel on Climate Change*, 741–866. https://doi.org/10.1017/CBO9781107415324.020

Held, I. M., & Soden, B. J. (2006). Robust responses of the hydrological cycle to global warming. *Journal of Climate*, *19*(21), 5686–1560. https://doi.org/10.1175/2010JCLI4045.1

Hoesly, R. M., Smith, S. J., Feng, L., Klimont, Z., Janssens-Maenhout, G., Pitkanen, T., et al. (2018). Historical (1750–2014) anthropogenic emissions of reactive gases and aerosols from the Community Emissions Data System (CEDS). *Geoscientific Model Development*, *11*(1), 369–408. https://doi.org/10.5194/gmd-11-369-2018

Hunke, E. C., Lipscomb, W. H., Turner, A. K., Jeffery, N., & Elliot, S. (2015). *CICE: The Los Alamos sea ice model documentation and software user's manual version 5.1* (Tech. Rep. No. LA-CC-06-012). Los Alamos National Laboratory.

Hwang, Y.-T., & Frierson, D. M. W. (2010). Increasing atmospheric poleward energy transport with global warming. *Geophysical Research Letters*, *37*(24). https://doi.org/10.1029/2010GL045440

Jungclaus, J. H., Bard, E., Baroni, M., Braconnot, P., Cao, J., Chini, L. P., et al. (2017). The PMIP4 contribution to CMIP6 – Part 3: The last millennium, scientific objective, and experimental design for the PMIP4 past1000 simulations. *Geoscientific Model Development*, *10*(11), 4005–4033. https://doi.org/10.5194/gmd-10-4005-2017

Kang, S. M., Held, I. M., Frierson, D. M. W., & Zhao, M. (2008). The response of the ITCZ to extratropical thermal forcing: Idealized slab-ocean experiments with a GCM. *Journal of Climate*, *21*(14), 3521–3532. https://doi.org/10.1175/2007JCLI2146.1

Kiehl, J. T. (2007). Twentieth century climate model response and climate sensitivity. *Geophysical Research Letters*, *34*(22), L22710. https://doi.org/10.1029/2007GL031383

Kravitz, B., Robock, A., Tilmes, S., Boucher, O., English, J. M., Irvine, P. J., et al. (2015). The Geoengineering Model Intercomparison Project Phase 6 (GeoMIP6): Simulation design and preliminary results. *Geoscientific Model Development*, *8*(10), 3379–3392. https://doi.org/10.5194/gmd-8-3379-2015

Kvalevåg, M. M., Samset, B. H., & Myhre, G. (2013). Hydrological sensitivity to greenhouse gases and aerosols in a global climate model. *Geophysical Research Letters*, *40*(7), 1432–1438. https://doi.org/10.1002/grl.50318

Lamarque, J. F., Bond, T. C., Eyring, V., Granier, C., Heil, A., Klimont, Z., et al. (2010). Historical (1850–2000) gridded anthropogenic and biomass burning emissions of reactive gases and aerosols: Methodology and application. *Atmospheric Chemistry and Physics*, *10*(15), 7017–7039. https://doi.org/10.5194/acp-10-7017-2010

Lawrence, D. M., Fisher, R. A., Koven, C. D., Oleson, K. W., Swenson, S. C., Bonan, G., et al. (2019). The Community Land Model version 5: Description of new features, benchmarking, and impact of forcing uncertainty. *Journal of Advances in Modeling Earth Systems*, *11*(12), 4245–4287. https://doi.org/10.1029/2018MS001583

Liu, X., Ma, P. L., Wang, H., Tilmes, S., Singh, B., Easter, R. C., et al. (2016). Description and evaluation of a new four-mode version of the Modal Aerosol Module (MAM4) within version 5.3 of the Community Atmosphere Model. *Geoscientific Model Development*, *9*(2), 505–522. https://doi.org/10.5194/gmd-9-505-2016

Ming, Y., Ramaswamy, V., & Persad, G. (2010). Two opposing effects of absorbing aerosols on global-mean precipitation. *Geophysical Research Letters*, *37*(13). https://doi.org/10.1029/2010GL042895

Mitchell, J. F. B., Wilson, C. A., & Cunnington, W. M. (1987). On CO_2 climate sensitivity and model dependence of results. *Quarterly Journal of the Royal Meteorological Society*, *113*(475), 293–322. https://doi.org/10.1002/qj.49711347517

Myhre, G., Forster, P. M., Samset, B. H., Hodnebrog, Ø., Sillmann, J., Aalbergsjø, S. G., et al. (2017). PDRMIP: A precipitation driver and response model intercomparison project—Protocol and preliminary results. *Bulletin of the American Meteorological Society*, *98*(6), 1185–1198. https://doi.org/10.1175/BAMS-D-16-0019.1

O'Gorman, P. A., Allan, R. P., Byrne, M. P., & Previdi, M. (2012). Energetic constraints on precipitation under climate change. *Surveys in Geophysics*, *33*(3), 585–608. https://doi.org/10.1007/s10712-011-9159-6

O'Gorman, P. A., & Muller, C. J. (2010). How closely do changes in surface and column water vapor follow Clausius–Clapeyron scaling in climate change simulations? *Environmental Research Letters*, *5*(2), 025207. https://doi.org/10.1088/1748-9326/5/2/025207

O'Gorman, P. A., & Schneider, T. (2009). The physical basis for increases in precipitation extremes in simulations of 21st-century climate change. *Proceedings of the National Academy of Sciences*, *106*(35), 14773–14777. https://doi.org/10.1073/pnas.0907610106

O'Neill, B. C., Tebaldi, C., Vuuren, D. P. V., Eyring, V., Friedlingstein, P., Hurtt, G., et al. (2016). The Scenario Model Intercomparison Project (ScenarioMIP) for CMIP6. *Geoscientific Model Development*, *9*(9), 3461–3482. https://doi.org/10.5194/gmd-9-3461-2016

Pandis, S. N., Harley, R. A., Cass, G. R., & Seinfeld, J. H. (1992). Secondary organic aerosol formation and transport. *Atmospheric Environment Part A. General Topics*, *26*(13), 2269–2282. https://doi.org/10.1016/0960-1686(92)90358-R

Peixoto, J. P., & Oort, A. H. (1992). *Physics of climate*. American Institute of Physics.

Previdi, M. (2010). Radiative feedbacks on global precipitation. *Environmental Research Letters*, *5*(2), 025211. https://doi.org/10.1088/1748-9326/5/2/025211

Ramanathan, V., Crutzen, P. J., Kiehl, J. T., & Rosenfeld, D. (2001). Aerosols, climate, and the hydrological cycle. *Science*, *294*(5549), 2119–2124. https://doi.org/10.1126/science.1064034

Richardson, T. B., Forster, P. M., Andrews, T., & Parker, D. J. (2016). Understanding the rapid precipitation response to CO_2 and aerosol forcing on a regional Scale. *Journal of Climate*, *29*(2), 583–594. https://doi.org/10.1175/JCLI-D-15-0174.1

Richter, I., & Xie, S. P. (2008). Muted precipitation increase in global warming simulations: A surface evaporation perspective. *Journal of Geophysical Research*, *113*(24), D24118. https://doi.org/10.1029/2008JD010561

Rodgers, K. B., Lee, S.-S., Rosenbloom, N., Timmermann, A., Danabasoglu, G., Deser, C., et al. (2021). Ubiquity of human-induced changes in climate variability. *Earth System Dynamics*, *12*(4), 1393–1411. https://doi.org/10.5194/esd-12-1393-2021

Samset, B. H., Myhre, G., Forster, P. M., Hodnebrog, Ø., Andrews, T., Faluvegi, G., et al. (2016). Fast and slow precipitation responses to individual climate forcers: A PDRMIP multimodel study. *Geophysical Research Letters*, *43*(6), 2782–2791. https://doi.org/10.1002/2016GL068064

Seinfeld, J. H., Bretherton, C., Carslaw, K. S., Coe, H., Demott, P. J., Dunlea, E. J., et al. (2016). Improving our fundamental understanding of the role of aerosol cloud interactions in the climate system. *Proceedings of the National Academy of Sciences*, *113*(21), 5781–5790. https://doi.org/10.1073/pnas.1514043113

Smith, R., Jones, P., Briegleb, B., Bryan, F., Danabasoglu, G., Dennis, J., et al. (2010). *The Parallel Ocean Program (POP) reference, manual ocean component of the Community Climate System Model (CCSM) and Community Earth System Model (CESM)* (LANL Tech. Report., Vol. 141, pp. 1–140).

Stott, P. A., Gillett, N. P., Hegerl, G. C., Karoly, D. J., Stone, D. A., Zhang, X., & Zwiers, F. (2010). Detection and attribution of climate change: A regional perspective. *Wiley Interdisciplinary Reviews: Climate Change*, *1*(2), 192–211. https://doi.org/10.1002/wcc.34

Trenberth, K. E., Dai, A., Rasmussen, R. M., & Parsons, D. B. (2003). The changing character of precipitation. *Bulletin of the American Meteorological Society*, *84*(9), 1205–1218. https://doi.org/10.1175/BAMS-84-9-1205

Utsumi, N., Seto, S., Kanae, S., Maeda, E. E., & Oki, T. (2011). Does higher surface temperature intensify extreme precipitation? *Geophysical Research Letters*, *38*(16). https://doi.org/10.1029/2011GL048426

van der Werf, G. R., Randerson, J. T., Giglio, L., Leeuwen, T. T. V., Chen, Y., Rogers, B. M., et al. (2017). Global fire emissions estimates during 1997–2016. *Earth System Science Data*, *9*(2), 697–720. https://doi.org/10.5194/essd-9-697-2017

van Marle, M. J., Kloster, S., Magi, B. I., Marlon, J. R., Daniau, A. L., Field, R. D., et al. (2017). Historic global biomass burning emissions for CMIP6 (BB4CMIP) based on merging satellite observations with proxies and fire models (1750–2015). *Geoscientific Model Development*, *10*(9), 3329–3357. https://doi.org/10.5194/gmd-10-3329-2017

Wallace, J. M., & Hobbs, P. V. (2006). *Atmospheric science: An introductory survey* (2nd ed.). Academic Press. https://doi.org/10.1016/C2009-0-00034-8

Zanchettin, D., Khodri, M., Timmreck, C., Toohey, M., Schmidt, A., Gerber, E. P., et al. (2016). The Model Intercomparison Project on the climatic response to Volcanic forcing (VolMIP): Experimental design and forcing input data for CMIP6. *Geoscientific Model Development*, *9*(8), 2701–2719. https://doi.org/10.5194/gmd-9-2701-2016

Reference From the Supporting Information

Wilks, D. S. (2016). "The stippling shows statistically significant grid points": How research results are routinely overstated and overinterpreted, and what to do about it. *Bulletin of the American Meteorological Society*, *97*(12), 2263–2273. https://doi.org/10.1175/BAMS-D-15-00267.1